Phase transformation of ZnMoO4 by localized thermal spike

D. C. Agarwal, D. K. Avasthi, S. Varma, Felipe Kremer, M. C. Ridgway, and D. Kabiraj

Citation: Journal of Applied Physics **115**, 163506 (2014); doi: 10.1063/1.4872259
View online: http://dx.doi.org/10.1063/1.4872259
View Table of Contents: http://scitation.aip.org/content/aip/journal/jap/115/16?ver=pdfcov
Published by the AIP Publishing

Phase transformation of $ZnMoO_4$ by localized thermal spike

D. C. Agarwal,[1] D. K. Avasthi,[1] S. Varma,[2] Felipe Kremer,[3] M. C. Ridgway,[3] and D. Kabiraj[1]
[1]*Inter-University Accelerator Center, Aruna Asaf Ali Marg, New Delhi 110067, India*
[2]*Institute of Physics, Sachivalaya Marg, Bhubaneswar 751005, India*
[3]*Australian National University, Canberra ACT 0200, Australia*

(Received 25 February 2014; accepted 11 April 2014; published online 23 April 2014)

We show that $ZnMoO_4$ remains in stable phase under thermal annealing up to 1000 °C, whereas it decomposes to ZnO and MoO_3 under transient thermal spike induced by 100 MeV Ag irradiation. The transformation is evidenced by X-ray diffraction (XRD), Raman spectroscopy, and X-ray photoelectron spectroscopy (XPS). Thin films of $ZnMoO_4$ were synthesized by thermal evaporation and subsequent annealing in oxygen ambient at 600 °C for 4 h. XRD results show that as the irradiation fluence increases, the peak related to $ZnMoO_4$ decreases gradually and eventually disappear, whereas peaks related to ZnO grow steadily up to fluence of 3×10^{12} ions/cm^2 and thereafter remain stable till highest fluence. This indicates that polycrystalline $ZnMoO_4$ film has transformed to polycrystalline ZnO thin film. The Raman lines related to $ZnMoO_4$ are observed to have disappeared with increasing irradiation fluence. XPS results show modification in bonding and depletion of Mo from near surface region after the ion irradiation. Cross-sectional transmission electron microscopy result shows the formation of ion track of diameter 12–16 nm. These results demonstrate that ion beam methods provide the means to control phase splitting of $ZnMoO_4$ to ZnO and MoO_3 within nanometric dimension along the ion track. The observation of phase splitting and Mo loss are explained in the framework of ion beam induced thermal spike formalism. © *2014 AIP Publishing LLC*. [http://dx.doi.org/10.1063/1.4872259]

I. INTRODUCTION

Oxide materials with complex crystal structures have been subjected to swift heavy ion (SHI) irradiation for the study of the theoretical aspect of latent track formation,[1,2] to introduce novel functionality,[3,4] search for materials to withstand extreme conditions,[5] formation of ordered structures,[6] formation of controlled pinning centers in high-Tc superconductors,[7] structural phase transition,[8] etc. In all the cases, the modifications are driven by unique feature of thermal spike (TS), generated along the ion-track during SHI irradiation. The passage of fast charged atomic particles (heavy ions) lead to extremely strong electronic excitations inside a narrow cylinder around each ion path. The initial interaction processes of the energy transfer from a high energy heavy ion to electrons bound to inner-shells take only 10^{-19}–10^{-17} s and slightly longer (about 10^{-16} s) for collective electronic excitations like formation of plasmons.[9] Hence, just after the passage of the SHI, the narrow cylindrical target zone coaxial with the ion path consists of two-component plasma of "cold" lattice atoms and "hot" electrons. The energy in the electronic sub-system is transferred to phonon sub-system by electron phonon coupling to initiate thermal spike. If the temperature of the thermal spike rises above melting point of the material, the core of the track melts which extends within few nanometers in radial direction and is potentially accompanied with vaporization and pressure wave generation to the surrounding materials. The melt quenches subsequently within time scale of pico- to nanoseconds and initiates re-solidification and defect recovery. The ultra fast collective atomic rearrangement drives the local atomic structure far from equilibrium that opens up different structural phase transition pathways, which end up with equilibrium and nonequilibrium states. The region within a track consisting of modified phases, which are few nanometers in diameter and tens of micrometers in length, opens up the possibility of novel materials modification in nanometer scale and the study of nonequilibrium phase transitions. There are various observations related to resultant structural properties within the track. This includes transition from crystalline to amorphous phase,[1] transition from one crystalline state to another crystalline state, like zirconia and hafnia transform from the monoclinic to the tetragonal phase,[10] whereas Y_2O_3 undergoes a cubic-to-monoclinic phase transformation.[11] Kluth *et al.*[12] have reported the formation of under dense cylindrical core of the track and over dense surrounding annular region in high energy Au and Xe irradiated thermally grown SiO_2 on Si. The superheated core where temperature is above the boiling point surrounded by solid boundary and rapid thermal quenching along with frozen-in pressure wave which originates from the center and propagates radially outwards is described to be the cause for such observation. Natural single-crystalline zircon ($ZrSiO_4$) when irradiated by Au and U of energy several GeV under high pressure up to 14 GPa decomposed to nano-crystals and there was nucleation of its high pressure phase, reidite. This phase formation is postulated to be due to pressure-pulse propagation around ion track.[8] In case of suboxide of Si (SiO_x) and Ge (GeO_x), SHI irradiation induced phase separation is reported. SiO_x and GeO_x phases separate into Si and SiO_2 and Ge and GeO_2, respectively.[13,14] Out of all the reports on SHI irradiation in oxide materials none report selective element loss. There are few reports where oxygen diffusion in molten track in Fe is reported to form iron oxide.[15,16] Just

opposite is observed by Li *et al*. in heavy ion irradiated Bi-2212 single crystals, where irradiation always increases hole density around the columnar defects due to oxygen deficiency. Oxygen ions, which are generated during thermal spike, are subsequently expelled from the columnar defects and the surplus of oxygen ions diffuses into the matrix.[17]

Here, we demonstrate that $ZnMoO_4$ when irradiated with 100 MeV Ag ions, phase segregates to ZnO-MoO_3 most probably along ion tracks due to thermal spike. As the ion fluence increases, the ion tracks overlap and finally entire thin film of $ZnMoO_4$ degenerate to mixed phase of polycrystalline ZnO and a glassy state of ZnO-MoO_3. Complementary analytical techniques like X-ray diffraction (XRD), Raman spectroscopy, X-ray photoelectron spectroscopy (XPS), and transmission electron microscopy (TEM) were used to establish it. Scheelite-structured $ZnMoO_4$ ternary oxide belongs to the wolframite-type metal molybdates with triclinic symmetry and has high potential applications in photoluminescence fields.[18,19] Moreover, $ZnMoO_4$ single crystals showed promising results as scintillating bolometers in high energy physics experiments.[20] At low temperatures (typically <20 mK for large bolometers), scintillating bolometers allow simultaneous detection of scintillation light and heat which provides a very powerful tool to identify the nature of the interacting particle and therefore to suppress background. Thus, a massive charged particle can be separated from an electron or γ due to the different light yield for the same amount of deposited heat. So the study of stability of this material under high energy ion irradiation can provide valuable information is an additional motivation for this work.

II. EXPERIMENTAL

$ZnMoO_4$ thin films were grown on Si substrates by thermal heating of ZnO in contact with Mo. At high temperature, ZnO reacts with Mo and forms $ZnMoO_x$ ($x < 4$) and evaporate to form thin film. The substrates were kept at room temperature (RT) and during evaporation the chamber pressure was 5×10^{-6} millibars. The thickness and deposition rate were monitored using a quartz crystal thickness monitor. The as-deposited films were amorphous in nature which transform to polycrystalline after annealed at 600 °C in oxygen ambient for 6 h. These annealed thin films were uniformly bombarded with 100 MeV Ag ions at RT with different fluences using 15UD Pelletron at IUAC, New Delhi. Grazing incidence XRD (GIXRD) spectra were recorded by Bruker D8 Advance diffractometer at a grazing incidence angle of 2°, using a CuK_α (1.5406 Å) source operating at 40 kV and 40 mA. Micro-Raman measurements of pristine and irradiated films on glass substrates were performed using Renishaw in-Via Raman microscope with Ar ion laser excitation at 514 nm. TEM was performed on cross-sectional samples using an FEI CM-300 operating at 300 kV.

III. RESULTS AND DISCUSSION

A. X-ray diffraction

X-ray diffraction spectra of pristine and irradiated $ZnMoO_4$ thin film samples are shown in Fig. 1. X-ray

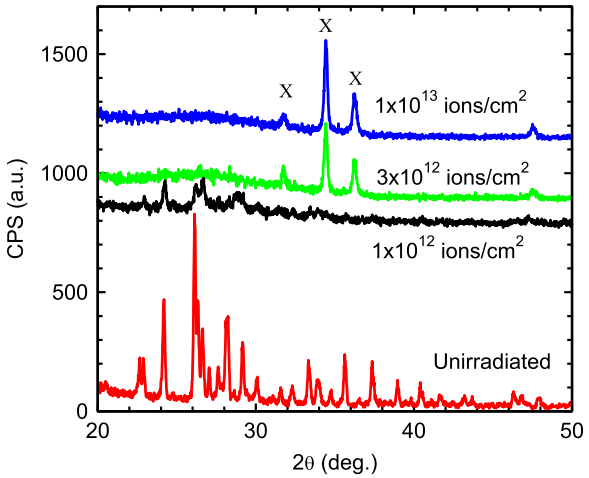

FIG. 1. XRD patterns of unirradiated $ZnMoO_4$ and irradiated at fluences of 1×10^{12}, 3×10^{12}, and 1×10^{13} ions/cm^2. The peaks marked by X are related to ZnO.

diffraction spectrum of pristine film reveals the formation of polycrystalline $ZnMoO_4$ phase and consistent with JCPDS 72-1486 [$ZnMoO_4$]. The structure of α-$ZnMoO_4$ crystals has been studied in detail by Abrahams[21] who reported the crystal structure as triclinic with a space group P1 and lattice parameters of $a = 09625$ nm, $b = 0.6965$ nm, $c = 0.8373$ nm, $\alpha = 103.28°$, $\beta = 96.30°$, and $\gamma = 106.72°$. This structure is complicated with Mo^{6+} ions occupying three non-equivalent positions being surrounded by four oxygen ions with approximately tetrahedral coordination. Zn^{2+} ions occupy sites with 5- and 6-fold coordination.

In Fig. 1, reflections related to zinc, zinc oxide, molybdenum, and molybdenum oxide phases are not observed in unirradiated sample. Ion beam irradiation of these films changes the structure gradually with increasing ion fluence and ZnO phase progressively evolved. Substantial decrease of the peaks related to $ZnMoO_4$ at low fluence of 1×10^{12} ions/cm^2 is observed. With further irradiation only three peaks with 2θ value of 31.5°, 34.4°, and 36.2° remain. These peaks are identified with (100), (002), and (101) reflections of ZnO. In Figs. 2(a) and 2(b), we plot the area under the (002) reflection of ZnO peak and corresponding FWHM. The area increases to maximum at ion fluence of 1×10^{13} ions/cm^2, then there is slow decrease with increasing fluence till the highest fluence of 7×10^{13} ions/cm^2. The FWHM follows the opposite trend, indicates the grain size is maximum at 1×10^{13} ions/cm^2 then potentially fragmentation of grains at higher irradiation fluences and associated increase of amorphous fraction at grain boundaries as reflected in decrease of area under the peak. Grain fragmentation is reported to be cause of increase in width of XRD peak of nonamorphizable material CaF_2 under thermal spike.[22] Minimal change in the position of the centroid is observed, which indicates that crystal structure is not modified due to irradiation.

B. Micro-Raman spectroscopy

The samples were further characterized by Raman spectroscopy to corroborate observed XRD results showing

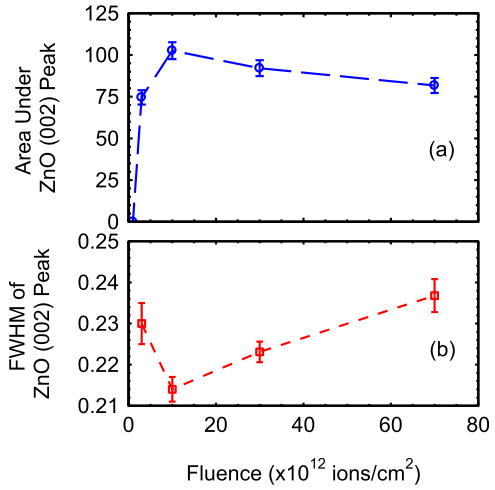

FIG. 2. (a) Area under ZnO (002) peak plotted against irradiation fluence. (b) FWHM of the same peak plotted against irradiation fluence. Connecting lines are guide to eye.

formation of polycrystalline ZnO after irradiation. The measured Raman spectra of pristine and irradiated $ZnMoO_4$ thin film samples are shown in Fig. 3. Raman spectrum of pristine film exhibits the characteristic nature of metal molybdate, and the peaks match well with the α-$ZnMoO_4$ formed in $ZnO\text{-}MoO_3\text{-}B_2O_3$ glass as reported by Aleksandrov *et al.*[23] Raman scattering spectra show several sharp peaks which match well with the result reported in Ref. 23, at 340, 370, 405, 787, 818, 849, 860, 882, 890, 930, 947, and 970 cm^{-1}. MoO_n polyhedra, i.e., MoO_4 tetrahedra and MoO_6 octrahedra, are known[24] to give strong Raman bands where band between 300 and 450 cm^{-1} is related to symmetric and anti-symmetric bending modes and between 750 and 1100 cm^{-1} is related to symmetric and anti-symmetric stretching modes. The peaks at 301, 520, and 618 cm^{-1} originate from Si substrate. After irradiation, all the Raman peaks disappear except a small hump at 330 cm^{-1} and a bigger one at 960 cm^{-1}. This is exactly opposite to what observed by Aleksandrov *et al.*,[23] where these two bands appear in amorphous glassy state and convert to sharp peaks when annealed to form crystalline α-$ZnMoO_4$. So we can infer that after irradiation, the crystalline phase converts to glassy amorphous phase of $ZnO\text{-}MoO_3$. The peak at 436.97 cm^{-1} evolved in irradiated samples, which is identified with E_2-high mode of ZnO, a characteristic feature of wurtzite structure of ZnO. The results indicate the irradiated thin films have two components: (i) crystalline ZnO phase, observed both in XRD and Raman spectroscopy and (ii) glassy amorphous phase $ZnO\text{-}MoO_3$ which is only observed by Raman spectroscopy.

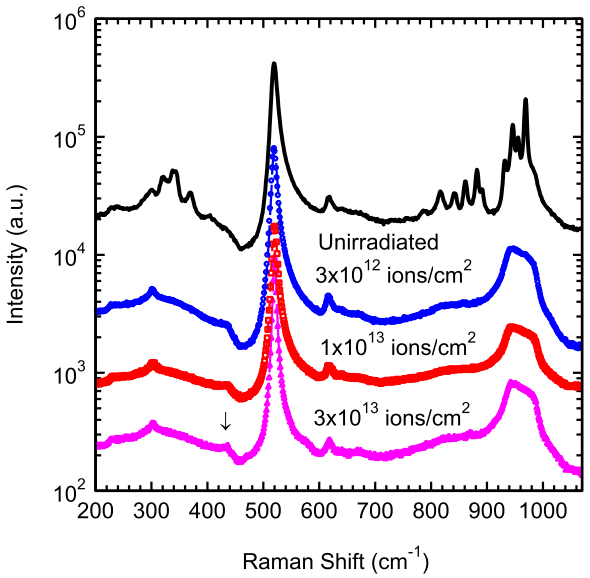

FIG. 3. Raman scattering spectra of unirradiated $ZnMoO_4$ and irradiated at fluences of 3×10^{12}, 1×10^{13}, and 3×10^{13} ions/cm^2. The peak at 436.97 cm^{-1} evolved in irradiated samples is shown by (↓).

C. X-ray photoelectron spectroscopy

X-ray photoelectron spectroscopy measurements have been performed to determine the elemental composition and oxidation state of elements. Carbon peak is used to calibrate the acquired spectra and the position of C 1s peak is located at binding energy of 284.6 eV. XPS spectra showing Mo 3d levels of pristine and irradiated samples are shown in Fig. 4(a). The doublet of Mo 3d peak appears at 232.4 and 235.6 eV, which corresponds to Mo $3d^{5/2}$ and $3d^{3/2}$,

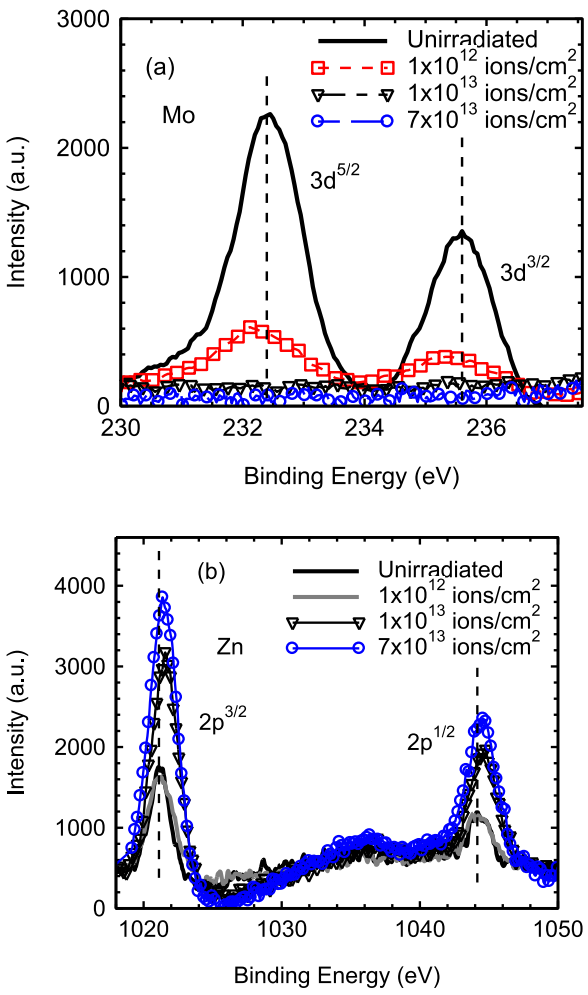

FIG. 4. XPS spectra of unirradiated and irradiated samples related to Mo 3d and Zn 2p are shown in (a) and (b), respectively.

respectively. As a result of spin-orbit splitting of Mo 3d level is giving rise to $3d^{5/2}$ and $3d^{3/2}$ levels with an energy separation of 3.2 eV, which is well matched with the present result. Near Gaussian shape of the Mo $3d^{5/2}$ peak indicates that most of Mo is present in +6 charge state.[25,26] Zn $2p^{3/2}$ and $2p^{1/2}$ peaks are present at 1021.1 eV and 1044.2 eV in the pristine sample as can be seen in Fig. 4(b). In irradiated samples, there is not much change in the shape of the peaks related to Zn. In the 1×10^{12} ions/cm^2 irradiated sample, there is substantial decrease of Mo peaks and shift to lower binding energy side. In samples irradiated at higher fluences, these Mo related features are absent. It confirms that there is loss of Mo at least up to the probing depth of XPS which is few nm only. Although after an irradiation with 1×10^{12} ions/cm^2, Zn $2p^{3/2}$ and $2p^{1/2}$ features display similar intensity as un-irradiated sample, they become stronger with increasing fluence. Moreover, at higher fluences (1×10^{13} and 7×10^{13} ions/cm^2), these Zn related peaks shift towards higher binding energies (see Fig. 4(b)). These shifts are consistent with the formation of ZnO at high fluences.

D. Transmission electron microscopy

Fig. 5 shows the cross section TEM of $ZnMoO_4$ film sample irradiated at 5×10^{10} ions/cm^2. The bright field image was obtained with the electron beam aligned to the Si ⟨110⟩ direction of the Si substrate, parallel to the $ZnMoO_4$/Si(001) interface. The apparent formation of ion tracks of diameter 12–16 nm is seen in TEM image. With average track diameter of 14 nm, the fluence at which the tracks start overlapping is $\sim 6 \times 10^{11}$ ions/cm^2, this is consistent with our XRD, Raman, and XPS results where we observe appreciable changes due to phase transition around this fluence.

The inelastic TS model (I-TS) is commonly used to describe swift heavy ion interactions with matter.[27] Within this framework, the ion irradiation is treated in a three-step model. In the first step, the electronic stopping power (S_e) of the ion is used to excite the target electron system. In Figure 5(b), along the ion track of 200 nm the average S_e is ~16 keV/nm. Then, the excited electrons propagate diffusively through the target. For a given material and S_e, the final effect strongly depends on the radial distribution of energy density. The energy stored in the electronic system is then transferred to the phonon system via electron–phonon coupling and finally leads to thermal spike. The electron-phonon coupling parameter g controls the flux of heat or energy from the electrons to the phonons per unit time and volume. This parameter governs the heating of the lattice and is thus a crucial quantity. The mathematical description is therefore based on a set of two coupled heat diffusion equations, one for the electron system and one for the phonon system.

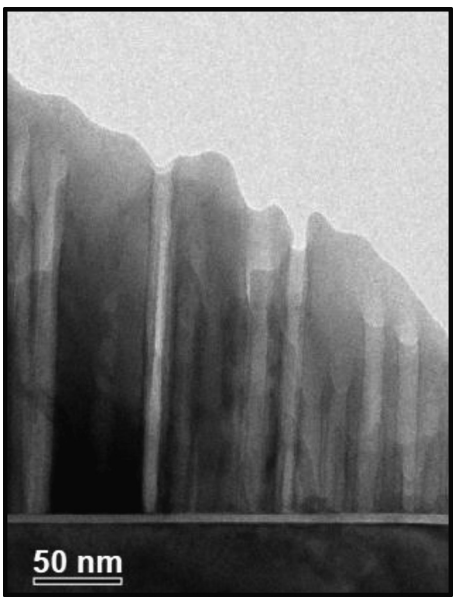

FIG. 5. Cross section TEM from irradiated at fluence of 5×10^{10} ions/cm^2.

A complete set of lattice thermodynamic parameters required to estimate the spike temperature using I-TS model is not available for $ZnMoO_4$ to best of our knowledge. The published experimental and theoretical understanding help us to explain that average electronic energy loss of 16 keV/nm deposited by 100 MeV Ag (~1 MeV/amu) can generate thermal spike to initiate track formation and material loss in $ZnMoO_4$ thin film. The effects of electronic stopping power in materials modification are non-liner and appear when the energy loss surpass threshold value. After stopping power exceeds threshold value, the track formation is observed in amorphizable material when track temperature is raised above melting point. On the other hand nonamorphizable materials, like materials with ionic bonding LiF, CaF_2, the track is observed when temperature exceeds vaporization temperature.[22]

Only limited experimental data are available on the electron-phonon coupling parameter for dielectrics, which is therefore often treated as a fitting parameter. It is related to electron-lattice interaction mean free path λ ($\lambda^2 = A/g$ with $A = 2$ J/s/cm/K) defined as the mean length of the energy diffusion within the electron system before the energy is transferred to lattice. The cutoff of the energy spread is restricted by the minimum ionization energy, that is, when electron energy is less than this energy. Here comes the link between the values of λ and band gap energy (E_g), which is the minimum ionization energy of electron in insulators. The values of λ for various insulators are evaluated by fitting experimentally observed track diameter and plotted against E_g in Ref. 1. The graph shows that, for E_g larger than 2.8 eV, there is only a slight decrease of λ from 5 to 4 nm. This indicates that in crystalline insulators the electron energy transfer towards the atoms happen in nearly same way.[28,29] $Y_3Fe_5O_{12}$ is a ferromagnetic insulator with band gap of 2.85 eV having complex garnet structure. $ZnMoO_4$ is a wide band gap insulator with $4.17\ \text{eV} < E_g < 5.35\ \text{eV}$ having complex molybdate structure with both having no congruent melt phase is expected to yield similar result under thermal spike.[30] It is reported that tracks appear in $Y_3Fe_5O_{12}$ when S_e is above 4 keV/nm and the sputtering above 16 keV/nm.[31,32] This experimental observation indicates that track temperature reached above vaporization temperature in $Y_3Fe_5O_{12}$ $S_e \sim 16$ keV/nm. With analogy given above, one can expect that electronic energy loss of 16 keV/nm is sufficient to raise the track temperature above melting point of $ZnMoO_4$.

We estimate the energy per atom for 100 MeV Ag irradiated $ZnMoO_4$ within cylindrical track volume of radius $R = 6.0$ nm and length 1 nm the mean deposited energy per atom can be evaluated as shown in Ref. 22

$$E_{atom=}S_e/(\pi \times R^2 \times N_{atom}). \quad (1)$$

In case of $ZnMoO_4$, atomic density N_{atom} is 6.9×10^{22} atoms/cm^3 and S_e is electronic energy loss at the corresponding beam energy, in this case it is 16 keV/nm. Equation (1) gives the value of $E_{atom} = 2.0$ eV/at. Our calculation shows that 100 MeV Ag irradiation of $ZnMoO_4$ which has melting point of $1007 \pm 2\,^{\circ}C$,[33,34] energy gain per atom $\sim$2.0 eV should raise track temperature to above melting point.

$ZnMoO_4$ incongruently melts to ZnO and MoO_3 at $\sim 1007 \pm 2\,^{\circ}C$[33,34] indicates that when thermal spike temperature exceeds this point such reaction occurs within the track volume. Very interesting of this system is that the one component of melt product MoO_3 has lower melting point ($\sim$795 °C) and the other component ZnO has much higher melting point (1975 °C) than $ZnMoO_4$.[32] The boiling point of MoO_3 is 1155 °C, which is close to the melting point of $ZnMoO_4$, may results in its ejection out of the track, which explains the loss of Mo in near surface region as observed in XPS measurement. In the subsurface region, during cooling of the ion track, the MoO_3 solidifies in amorphous glassy phase so could not be observed in XRD spectrum (Fig. 1) but appeared as humps in Raman spectroscopy (Fig. 3). On the other hand, after phase separation during thermal spike, ZnO with inter-atomic bonding being highly ionic in nature remain in polycrystalline form as shown in XRD and Raman spectroscopy (Figs. 1 and 3).

IV. CONCLUSIONS

We have demonstrated that phase segregation of $ZnMoO_4$ takes place due to 100 MeV Ag irradiation. The proposed mechanism of formation of glassy ZnO-MoO_3 phase is due to incongruent melting of $ZnMoO_4$ during transient molten phase. ZnO solidifies in polycrystalline form as observed by XRD. XPS measurement indicates loss of Mo from near surface region is attributed to vaporization of MoO_3, as its boiling temperature is close to the melting point of $ZnMoO_4$.

ACKNOWLEDGMENTS

We thankfully acknowledge Pelletron group, Inter-University Accelerator Centre for delivering stable beam for irradiation. We also acknowledge Professor Anushree Roy, IIT Kharagpur for micro-Raman measurement and Mr. Santosh Choudhury of Institute of Physics, Bhubaneswar who has taken XPS.

[1] M. Toulemonde, Ch. Dufour, A. Meftah, and E. Paumier, Nucl. Instrum. Methods Phys. Res., Sect. B **166–167**, 903 (2000).
[2] M. Toulemonde, W. J. Weber, G. Li, V. Shutthanandan, P. Kluth, T. Yang, Y. Wang, and Y. Zhang, Phys. Rev. B **83**, 054106 (2011).
[3] K.-i. Nomura, M. Fujimaki, K. Awazu, and T. Komatsubara, J. Vac. Sci. Technol., A **29**, 051402 (2011).
[4] A. Dallanora, T. L. Marcondes, G. G. Bermudez, P. F. P. Fichtner, C. Trautmann, M. Toulemonde, and R. M. Papaléo, J. Appl. Phys. **104**, 024307 (2008).
[5] J. Zhang, M. Lang, R. C. Ewing, R. Devanathan, W. J. Weber, and M. Toulemonde, J. Mater. Res. **25**, 1344 (2010).
[6] W. Bolse, Nucl. Instrum. Methods Phys. Res., Sect. B **244**, 8 (2006).
[7] Y. Zhu, Z. X. Cai, R. C. Budhani, M. Suenaga, and D. O. Welch, Phys. Rev. B **48**, 6436 (1993).
[8] U. A. Glasmacher, M. Lang, H. Keppler, F. Langenhorst, R. Neumann, D. Schardt, C. Trautmann, and G. A. Wagner, Phys. Rev. Lett. **96**, 195701 (2006).
[9] G. Schiwietz, K. Czerski, M. Roth, F. Staufenbiel, and P. L. Grande, Nucl. Instrum. Methods Phys. Res., Sect. B **226**, 683 (2004).
[10] A. Benyagoub, Phys. Rev. B **72**, 094114 (2005).
[11] S. Hémon, V. Chailley, E. Dooryhee, C. Dufour, F. Gourbilleau, F. Levesque, and E. Paumier, Nucl. Instrum. Methods Phys. Res., Sect. B **122**, 563 (1997).
[12] P. Kluth, C. S. Schnohr, O. H. Pakarinen, F. Djurabekova, D. J. Sprouster, R. Giulian, M. C. Ridgway, A. P. Byrne, C. Trautmann, D. J. Cookson, K. Nordlund, and M. Toulemonde, Phys. Rev. Lett. **101**, 175503 (2008).
[13] W. M. Arnoldbik, N. Tomozeiu, E. D. van Hattum, R. W. Lof, A. M. Vredenberg, and F. H. P. M. Habraken, Phys. Rev. B **71**, 125329 (2005).
[14] Y. Batra, D. Kabiraj, S. Kumar, and D. Kanjilal, J. Phys. D: Appl. Phys. **40**, 4568 (2007).
[15] T. Roller and W. Bolse, Phys. Rev. B **75**, 054107 (2007).
[16] D. K. Avasthi, W. Assmann, A. Tripathi, S. K. Srivastava, S. Ghosh, F. Grüner, and M. Toulemonde, Phys. Rev. B **68**, 153106 (2003).
[17] M. Li, C. J. van der Beek, M. Konczykowski, H. W. Zandbergen, and P. H. Kes, Phys. Rev. B **66**, 014535 (2002).
[18] R. Graser, E. Pitt, A. Scharmann, and G. Zimmerer, Phys. Status Solidi B **69**, 359 (1975).
[19] J. Ryu, S. Koo, J. Yoon, C. Lim, and K. Shim, Mater. Lett. **60**, 1702 (2006).
[20] J. W. Beeman *et al.*, Phys. Lett. B **710**, 318 (2012).
[21] S. C. Abrahams, J. Chem. Phys. **46**, 2052 (1967).
[22] M. Toulemonde, A. Benyagoub, C. Trautmann, N. Khalfaoui, M. Boccanfuso, C. Dufour, F. Gourbilleau, J. J. Grob, J. P. Stoquert, J. M. Costantini, F. Haas, E. Jacquet, K.-O. Voss, and A. Meftah, Phys. Rev. B **85**, 054112 (2012).
[23] L. Aleksandrov, T. Komatsu, R. Iordanova, and Y. Dimitriev, Opt. Mater. **33**, 839 (2011).
[24] C. Luz-Lima, G. D. Saraiva, A. G. S. Filho, W. Paraguassu, P. T. C. Freire, and J. M. Filho, J. Raman Spectrosc. **41**, 576 (2010).
[25] X. Fan, G. Fang, P. Qin, N. Sun, N. Liu, Q. Zheng, F. Cheng, L. Yuan, and X. Zhao, J. Phys. D: Appl. Phys. **44**, 045101 (2011).
[26] M. F. Al-Kuhaili, S. M. A. Durrani, I. A. Bakhtiari, and A. M. Al-Shukri, Opt. Commun. **283**, 2857 (2010).
[27] M. Toulemonde, C. Dufour, and E. Paumier, Phys. Rev. B **46**, 14362 (1992).
[28] G. Szenes, Phys. Rev. B **51**, 8026 (1995).
[29] G. Szenes, Phys. Rev. B **52**, 6154 (1995).
[30] D. Spassky, A. Vasil'ev, I. Kamenskikh, V. Kolobanov, V. Mikhailin, A. Savon, L. Ivleva, I. Voronina, and L. Berezovskaya, Phys. Status Solidi A **206**(7), 1579–1583 (2009).
[31] A. Meftah, F. Brisard, J. M. Costantini, M. Hage-Ali, J. P. Stoquert, F. Studer, and M. Toulemonde, Phys. Rev. B **48**, 920 (1993).
[32] A. Meftah, M. Djebarra, J. P. Stoquert, F. Studer, and M. Toulemonde, Nucl. Instrum. Methods Phys. Res., Sect. B **107**, 242 (1996).
[33] T. Söhnel, W. Reichelt, H. Oppermann, Hj. Mattaush, and A. Simon, Z. Anorg. Allg. Chem. **622**, 1274 (1996).
[34] L. I. Ivleva, I. S. Voronina, L. Yu. Berezovskaya, P. A. Lykov, V. V. Osiko, and L. D. Iskhakova, Crystallogr. Rep. **53**, 1087 (2008).